Steps toward Identifying PAHs:
A Summary of Some Recent Results

Douglas M. Hudgins† and L. J. Allamandola

Astrophysics Branch, NASA Ames Research Center, Mountain View, CA, USA

Abstract. Based on over two decades of experimental, observational, and theoretical studies by scientists around the world, it is now widely accepted that the composite emission of mixtures of vibrationally-excited PAHs and PAH ions can accommodate the general pattern of band positions, intensities, and profiles observed in the discrete IR emission features of carbon-rich interstellar dust, as well as the variations in those characteristics. These variations provide insight into the detailed nature of the emitting PAH population and reflect conditions within the emitting regions giving this population enormous potential as probes of astrophysical environments. Moreover, the ubiquity and abundance of this material has impacts that extend well beyond the IR.

In this paper we will examine recent, combined experimental, theoretical, and observational studies that indicate that nitrogen-substituted PAHs represent an important component of the interstellar dust population, and we will go on to explore some of the ramifications of this result. We will also explore the results of recent experimental studies of the strong, low-lying electronic transitions of ionized PAH ions in the near-IR (0.7–2.5 μm) and explore the role that these transitions might play in pumping the PAH IR emission in regions of low excitation.

Keywords. astrochemistry — infrared: ISM — ISM: molecules — ISM: dust — ISM: lines and bands — methods: laboratory — molecular processes — techniques: spectroscopic

1. Introduction

Most interstellar objects with associated gas and dust exhibit a series of strong infrared emission features near 3.3, 6.2, 7.7, 8.6, and 11.2 μm which are generally attributed to polycyclic aromatic hydrocarbons (PAHs) and related molecular materials (e.g., Allamandola, Tielens, & Barker 1989; Puget & Leger 1989; Cox & Kessler 1999). Within the framework of this PAH model, the interstellar features arise from the combined emission of a complex mixture of PAH species that together comprise the molecular component of the carbon-rich interstellar dust population. The wide acceptance currently enjoyed by the interstellar PAH model is based on more than a decade of laboratory measurements and theoretical calculations (e.g., Vala *et al.* 1994; Hudgins & Allamandola 1995; Szczepanski *et al.* 1995; Langhoff 1996; Bauschlicher & Langhoff 1997; Pauzat & Ellinger 2001; Kim & Saykally 2002; Mattioda *et al.* 2003; Oomans *et al.* 2003; and references therein), which have shown that models based on the composite spectra of PAHs and PAH cations can accommodate the general pattern of band positions, intensities, and profiles observed in the interstellar IR emission spectra as well as the variations in those characteristics (e.g., Allamandola, Hudgins, & Sandford 1999; Van Kerckhoven *et al.* 2000; Hony *et al.* 2001; Verstraete *et al.* 2001; Bakes, Tielens, & Bauschlicher 2001; Bakes *et al.* 2001; Draine & Li 2001; Li & Draine 2001; Pech, Joblin, & Boissel 2002). Overall, that work indicates that the interstellar 3.3 μm band and, to a lesser extent, the

† Present address: Universe Division, Mail Suite 3W39, NASA Headquarters, 300 E St. SW, Washington DC 20546, USA; email: Douglas.M.Hudgins@nasa.gov

11.2 μm band are dominated by the emission of neutral PAHs, whose most prominent bands fall in these regions. Conversely, the interstellar bands in the 6–9 μm are dominated by the emission of ionized PAHs, whose most prominent bands fall in this region and are an order of magnitude more intense than those of the analogous neutral species.

Nevertheless, the agreement between the interstellar emission spectra and model spectra based on the latest experimental and theoretical data is not perfect. However, the discrepancies between observations and models have the potential to provide as much insight into the astrophysical problem as the agreements. For example, one issue that has emerged from the most recent analyses concerns the enigmatic position of the nominal 6.2 μm emission band, attributed to the CC stretching vibrations of interstellar PAH cations. Laboratory measurements and theoretical calculations of the IR spectra of a wide range of PAH cations have shown that the dominant CC stretching features of those species consistently fall at somewhat longer wavelengths than does the interstellar feature. This discrepancy is illustrated in Figure 1, which compares a typical interstellar emission spectrum to a simple PAH model in the 6.2 μm region. Hudgins & Allamandola (1999) noted this discrepancy, but also found that, for the small PAH cations ($N_C \leqslant 24$ C atoms) in their dataset, the dominant CC stretching bands shifted towards shorter wavelengths as molecular size increased, suggesting that the position of the interstellar emission band might be indicative of the size of the dominant emitters. However, as illustrated by the plot of band position verses molecular size shown in Figure 1(b), more recent experimental and theoretical studies of larger species show that this trend does not hold for larger PAHs. Instead, the positions of the CC stretching features of PAHs larger than about 30 C atoms are insensitive to molecular size and tend to cluster around 6.3 μm. Thus, molecular size alone is not sufficient to explain the 6.2 μm position of the interstellar band.
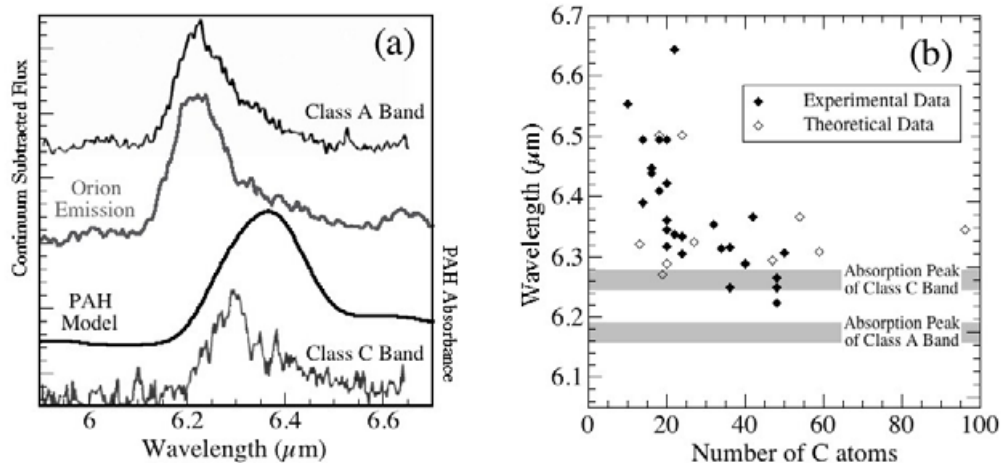

Figure 1. (a) A comparison of a typical 6.2 μm interstellar emission band (Orion) to a simple PAH model illustrating that the CC stretching features of PAH cations consistently fall at somewhat longer wavelengths than the interstellar feature. The canonical Class A and Class C emission bands identified by Peeters $et\ al.$ (see text) are also included (plot adapted from Peeters $et\ al.$ 2002). (b) A plot illustrating the variation in the position of the dominant CC stretching absorption feature as a function of molecular size for 3 dozen PAH cations. Filled diamonds indicate experimental data; open diamonds represent theoretical data. The bars indicate the $expected\ absorption$ positions (see text) of the Class A and Class C emission components (plot adapted from Hudgins, Bauschlicher, & Allamandola 2005).

Further light was shed on the precise nature of this discrepancy by the detailed observational work of Peeters *et al.* (2002). In that study, the authors showed that the nominal interstellar 6.2 μm band is actually a composite of two bands, one centered near 6.2 μm and one centered near 6.3 μm. Variations in the relative contributions of these two components give rise to variations in both the position and profile of the composite feature. Bands dominated by the shorter wavelength component (by far the most common case) fall at an average position of 6.215 μm and are designated "Class A" bands. Bands that are dominated by the longer wavelength component fall at an average position of 6.295 μm and are designated "Class C" bands. "Class B" bands are a composite of Classes A and C and exhibit intermediate positions and compound profiles. The canonical Class A and Class C bands isolated by Peeters *et al.* (2002) are also shown in Figure 1(*a*) for reference. For the purpose of direct comparison, the positions of the Class A and Class C bands are also indicated in Figure 1(*b*), adjusted to compensate for the expected *ca.* 10 cm^{-1} redshift between emission and absorption peak frequencies (Joblin *et al.* 1995). Based on these data, Peeters *et al.* concluded that while moderately-sized PAH cations ($N_C \geqslant 40$ C atoms) might accommodate the position of 6.3 μm Class C component, the origin of the 6.2 μm Class A component remained anomalous within the framework of the PAH model.

2. The Effects of N Substitution on the IR Spectrum of PAHs

In an effort to explore the origin of this and other discrepancies in detail between the interstellar emission and the spectroscopic properties of PAHs, we have continued to expand our studies to encompass new and different PAH-related species – species with structural or compositional characteristics that distinguish them from the other aromatic species in the database and which might give rise to distinctive spectroscopic properties. Among these are polycyclic aromatic nitrogen heterocycles (PANHs), compounds that incorporate one or more atoms of nitrogen within their aromatic carbon skeleton. Detailed accounts of these studies and their astrophysical implications are available in the literature (Mattioda *et al.* 2003; Hudgins, Bauschlicher, & Allamandola 2005, hereafter HBA 05) and will only be summarized here.

The structures of some representative examples of this class of aromatic compound that have been considered in our studies are shown in Figure 2. To specify the position of N-substitution within the C skeletons of the various molecules, we have adopted the following convention: position 1 corresponds to replacement of a CH group on the periphery of the molecule with an N atom. Since this substitution places the N atom on the edge (or exterior) of the C skeleton, we refer to this as an *exoskeletal* PANH. Substitution at positions designated 2, 3, 4, etc. corresponds to replacing a C atom that is 1, 2, 3, etc. bonds removed from the edge (*i.e.* the nearest CH group), respectively. Such an N atom is necessarily buried within the carbon skeleton of the molecule, and the molecule is referred to as an *endoskeletal* PANH.

The studies of PANH cations summarized here are based on a combination of laboratory work and theoretical calculations. Since an N atom is isoelectronic with a CH group, neutral exoskeletal PANHs have a closed-shell electronic structure (all electrons are paired). Samples of many such molecules are stable and can be obtained for experimental work. Conversely, an N atom contains one more electron than does a C atom, so neutral endoskeletal PANHs have a radical (open shell) electronic structure. Such species are not stable and are inaccessible by current experimental techniques. Thus, the same Density Functional Theory techniques that have previously been applied to the analyses
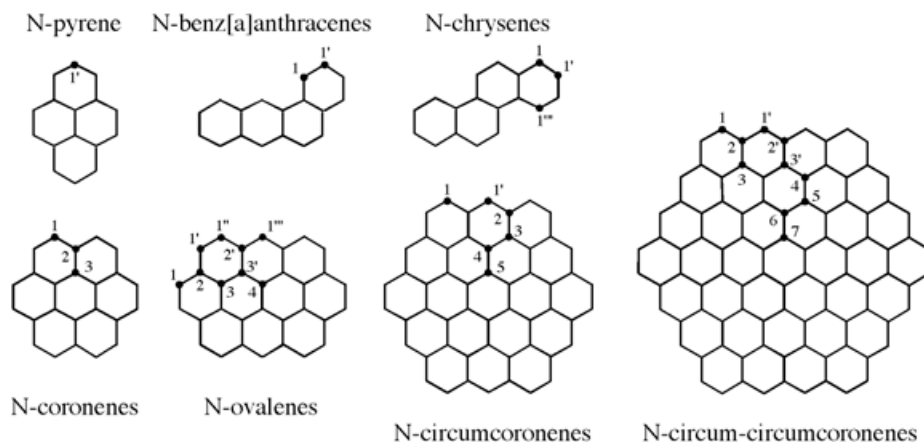
Figure 2. Generalized structures of the PANH species discussed in this manuscript. The numbers identify the possible unique positions for N atom substitution in the structure and are assigned as described in the text.

of the IR spectroscopic PAHs and their cations, have been particularly crucial to the study of endoskeletal PANHs and their cations.

Table 1 lists the positions of the dominant bands in the CC stretching region for the PANH cations shown in Figure 2 as well as their shifts from the analogous unsubstituted PAH cations. Inspection of the data for the exoskeletal PANH cations (those with a "1N" prefix) reveals that, although N-substitution is sometimes accompanied by a small blueshift, that blueshift is too modest to bring the dominant band in the region into agreement with the 6.215 μm Class A component of the interstellar spectra. However, the story changes as we move the N atom into the interior of the carbon skeleton. Consider, for example, the N-substituted coronenes shown in Table 1. Incorporation of an N atom at the endoskeletal 2 or 3 positions shifts the dominant CC stretching feature to 6.177 μm and 6.184 μm, respectively. This is precisely the absorption position required to accommodate the Class A emission component when one takes into account the 10 cm^{-1} (*ca.* 0.04 μm at 6.2 μm) redshift between emission and absorption peak frequencies (Joblin *et al.* 1995).

The effect of N substitution on the position of the dominant CC stretching band is illustrated graphically in Figure 3(a) which shows a spectral rendering of the calculated spectrum of the series of N-circumcoronenes in the 6.2 μm region compared to the canonical Class A and C bands of Peeters *et al.* (2002). That figure shows that as the substitutional position of the N atom moves deeper into the C skeleton of the molecule, the dominant CC stretching feature shifts to shorter wavelengths, agreeing well with the position of the Class A interstellar feature for the innermost endoskeletal positions. The data for the N-ovalene and N-circum-circumcoronene cations in Table 1 shows that a significant blueshift of the CC stretching band is a general characteristic of endoskeletal PANH cations. This effect is quantified in Figure 3(b) which shows a plot of the position of the dominant CC stretching band as a function of N substitution position for the four large, condensed cations in Table 1. It is interesting to note that the impact of N atom substitution (*i.e.* the slope of each curve in Figure 3b) is dependent on molecular size – the larger the molecule, the more modest the effect. Additional studies detailed elsewhere (HBA 05) have shown that, for species larger than 30 or so C atoms, 2 or more endoskeletal N atoms are required to achieve the full measure of the blueshift needed to accommodate the interstellar Class A band. Based on that result, it is estimated that

Table 1. Molecular characteristics and positions of the dominant 6.2 μm bands for a range of singly-substituted PANHs compared to their parent hydrocarbons.

Species	Formula	Exo-/endo-skeletal N	Dominant 6.2 μm CC Stretching Band Position			
			λ (μm)	$\Delta\lambda$ (μm)	$\tilde{\nu}$ (cm^{-1})	$\Delta\tilde{\nu}$ (cm^{-1})
Experimental Measurements[a]						
Pyrene Cation	$C_{16}H_{10}^{+}$	-	6.439		1553	
1'N-pyrene^{+}	$C_{15}H_{9}N^{+}$	exo	6.456	+0.017	1549	-4
Benz[a]anthracene cation	$C_{18}H_{12}^{+}$	-	6.494		1540	
1N-benzanthracene^{+}	$C_{17}H_{11}N^{+}$	exo	6.502	+0.008	1538	-2
1'N-benzanthracene^{+}	↓	exo	6.532	+0.038	1531	-9
Chrysene Cation	$C_{18}H_{12}^{+}$	-	6.410		1560	
1N-chrysene^{+}	$C_{17}H_{11}N^{+}$	exo	6.414	+0.004	1559	-1
1'N-chrysene^{+}	↓	exo	6.439	+0.029	1553	-7
1'''N-chrysene^{+}	↓	exo	6.394	-0.016	1564	+4
Theoretical Calculations[a]						
Coronene cation	$C_{24}H_{12}^{+}$	-	6.441	-	1553	-
1N-coronene$^{+,c}$	$C_{23}H_{12}N^{+}$	exo	6.254	-0.187	1599	+35
2N-coronene^{+}	↓	endo	6.177[b]	-0.222	1619[a]	+55
3N-coronene^{+}	↓	endo	6.184	-0.257	1617	+64
Ovalene cation	$C_{32}H_{14}^{+}$	-	6.415	-	1559	-
1N-ovalene$^{+,c}$	$C_{31}H_{14}N^{+}$	exo	6.320	-0.095	1582	+23
1'N-ovalene$^{+,c}$		exo	6.332	-0.083	1579	+20
1''N-ovalene$^{+,c}$		exo	6.324	-0.091	1581	+22
1'''N-ovalene$^{+,c}$		exo	6.268	-0.147	1595	+36
2N-ovalene^{+}		endo	6.267	-0.148	1596	+37
2'N-ovalene^{+}		endo	6.277	-0.138	1593	+34
3N-ovalene^{+}		endo	6.243	-0.172	1602	+43
3'N-ovalene^{+}		endo	6.231	-0.184	1605	+46
4N-ovalene^{+}		endo	6.202	-0.213	1612	+53
Circumcoronene cation	$C_{54}H_{18}^{+}$	-	6.365	-	1571	-
1N-circumcoronene$^{+,c}$	$C_{53}H_{14}N^{+}$	exo	6.252[d]	-0.113	1600[c]	+29
1'N-circumcoronene$^{+,c}$		exo	6.309	-0.056	1585	+14
2N-circumcoronene^{+}		endo	6.250	-0.115	1600	+29
3N-circumcoronene^{+}		endo	6.234	-0.131	1604	+33
4N-circumcoronene^{+}		endo	6.215	-0.15	1609	+38
5N-circumcoronene^{+}		endo	6.211	-0.154	1610	+39
Circum-circumcoronene cation	$C_{96}H_{24}^{+}$	-	6.345	-	1576	-
2N-circumcircumcor^{+}	$C_{95}H_{24}N^{+}$	endo	6.262	-0.083	1597	+21
2'N-circumcircumcor^{+}		endo	6.266	-0.079	1596	+20
3N-circumcircumcor^{+}		endo	6.305	-0.040	1586	+10
3'N-circumcircumcor^{+}		endo	6.281	-0.064	1592	+16
4N-circumcircumcor^{+}		endo	6.277	-0.068	1593	+17
5N-circumcircumcor^{+}		endo	6.256	-0.089	1599	+23
6N-circumcircumcor^{+}		endo	6.258	-0.087	1598	+22
7N-circumcircumcor^{+}	↓	endo	6.242	-0.103	1602	+26

[a] — experimental data correspond to argon matrix-isolation measurements from Mattioda et al. 2003; theoretical data were computed using density functional theory at the B3LYP/4-31G and are taken from Hudgins, Bauschlicher, and Allamandola 2005.

[b] — shorter wavelength component of a doublet; a longer wavelength component with similar intensity falls at a position of 6.274 μm (1594 cm^{-1}).

[c] — closed-shell, protonated form of the exoskeletal PANH cation. See discussion in text (Hudgins, Bauschlicher, and Allamandola 2005).

[d] — shorter wavelength component of a doublet; a longer wavelength component with similar intensity falls at a position of 6.452 μm (1550 cm^{-1}).
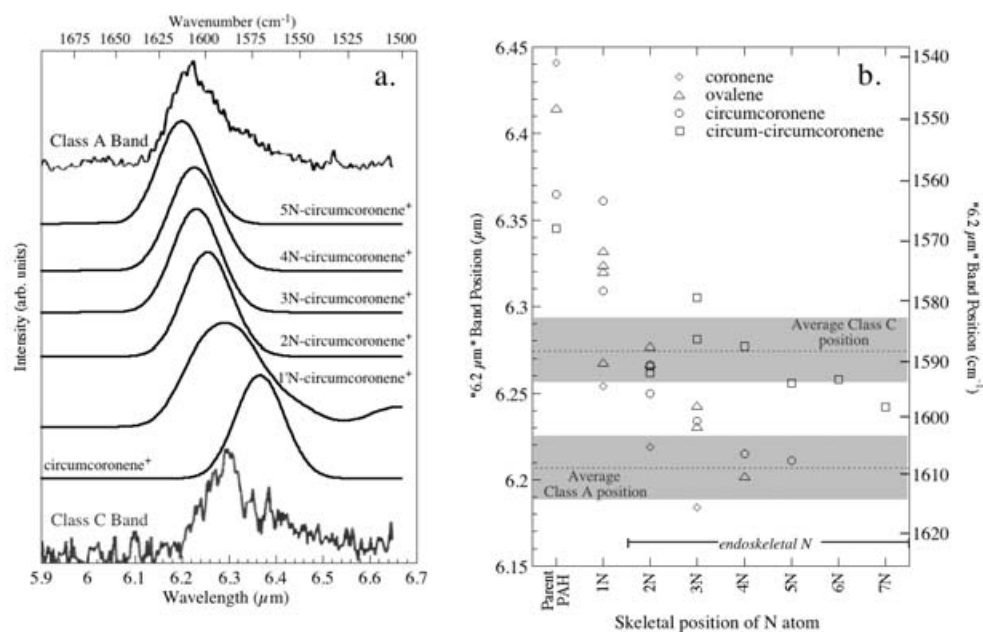
Figure 3. This figure illustrates the spectroscopic effects of endoskeletal N atom substitution on the position of the dominant CC stretching modes of PANH cations (HBA 05). The structures of the species are shown in Figure 2 above. (*a*) A comparison of the Class A and Class C 6.2 μm emission components to a spectral rendering of the theoretical results for various possible N-circumcoronene cations. The plot is adapted from HBA 05 and details can be found therein. (*b*) The position of the CC stretching band plotted as a function of N substitution position. All data calculated using DFT at the B3LYP/4-31G level.

the C/N ratio in the interstellar PANH population can be no more than ~ 30, and that, consequently, approximately 1%–5% of the available cosmic N is tied up in PAHs.

Finally, not only are endoskeletal PANH cations the first species found that can accommodate the 6.215 m Class A emission band identified by Peeters *et al.*, a strong case can be made that they are also by far the most likely origin of this feature. That case is discussed in detail in HBA 05 and is beyond the scope of this paper. However, in a nutshell, focused theoretical analyses of key representative species in conjunction with the chemical and astrophysical constraints of the problem can be used to rule out or render unlikely such alternatives as larger and or different PAH species, dehydrogenated/superhydrogenated PAHs, aromatic heterocycles involving elements other than N, and PAH-metal atom complexes (*i.e.* "metallocenes") as the origin of the anomalous Class A emission band. Consequently, all the available evidence indicates that endoskeletal PANHs are unique in their capacity to accommodate the Class A 6.2 μm emission component and that this feature provides a tracer of N in the interstellar PAH population.

3. The Rotational Spectroscopy of PANHs

Although the last two decades have seen a renaissance in our understanding of the IR spectroscopic properties of PAHs, the spectroscopic properties of PAHs in that other great realm of astronomical molecular spectroscopy – the radio region – have received relatively little attention. There are several significant challenges to detecting the radio emission

from specific PAH species in astronomical environments. First, although PAHs as a family are the most abundant interstellar molecules, the population consists of an enormous number of discrete molecular species. It is unclear whether any one particular PAH species will be present in sufficient abundance to permit unambiguous identification. The problem is further compounded by the extreme complexity of the rotational spectra of all but the most symmetric PAH species. Because of this complexity, the total energy emitted at radio frequencies will, in general, be distributed over a large number of weak lines rather than concentrated into a few stronger ones. Happily, with advances in observational technologies and techniques at radio wavelengths, the radio frequency spectroscopy of PAHs is receiving increased attention as evidenced by the work of Thorwirth and others highlighted elsewhere in this volume.

Another obstacle to studies of the pure rotational spectroscopy of interstellar PAHs has been the fact that pure PAHs tend to have relatively small dipole moments and, consequently, weak rotational transition. PANHs, on the other hand, possess significant dipole moments and would be expected to exhibit intrinsically stronger rotational transitions. Given the evidence indicating that N-substituted aromatic compounds play an important role in the interstellar PAH population, these species may represent attractive targets for an astronomical search. Toward this end, the dipole moments and rotational constants have been calculated at the B3LYP/4–31G level of theory and are tabulated in Tables 2 and 3, respectively. In those tables, the rotational axes of each molecule are identified as a, b, and c on the basis of the moment of inertia, I, about each axis and according to the convention $I_a < I_b < I_c$. Calibration calculations at the same level of theory for the benzene molecule yield rotational constants that are accurate to within 1%. Thus, while rotational constants such as those listed in Table 2 are insufficient to calculate precise rotational line positions, they are sufficient to constrain the strengths and wavelength regions in which PANH rotational transitions are expected.

Given the enormous number of PANH structures possible and the wide range of rotational constants they encompass, interstellar PANHs should produce a very dense forest of lines over a very broad spectral range. For example, a mixture of PANHs up to a size of circum-circumcoronene at 100 K are expected to emit in a pseudo-continuum between about 0 and 40 GHz. On the other hand, given the large dipole moments associated with PANHs, it may also be possible to distinguish the rotational emission lines of interstellar PANHs amongst the forest of molecular rotational lines observed in cold, dark molecular clouds where the low ambient temperatures ($T_{\mathrm{gas}} \simeq 10$ K) collapse the rotational energy into a relatively small number of transitions. Furthermore, it may be that there are some PANH species which possess large dipole moments and have a high enough degree of symmetry that the number of substitutional isomers is sufficiently small that these species could have unusually intense radio lines.

Table 2. Calculated rotational constants for the cations of several singly-substituted PANHs.

Cations	Rotational Constants (GHz)			Cations	Rotational Constants (GHz)		
	R_a	R_b	R_c		R_a	R_b	R_c
1'N-pyrene	1.027	0.551	0.359	N-coronenes	0.334– 0.337	0.331– 0.336	0.166– 0.168
1N-benz[a]anthracene	1.166	0.262	0.214				
1'N-benz[a]anthracene	1.173	0.256	0.210	N-ovalenes	0.238	0.148	0.091
1N-chrysene	1.279	0.261	0.217	N-circumcoronenes	0.066	0.066	0.033
1'N-chrysene	1.283	0.259	0.216	N-circum- circumcoronenes	0.021	0.021	0.011
1'''N -chrysene	1.270	0.265	0.220				

Table 3. Calculated dipole moments for the cations of several singly-substituted PANHs.

Species	Dipole Moments (Debye)			Species	Dipole Moments (Debye)		
	μ_a	μ_b	μ		μ_a	μ_b	μ
N-pyrene cation, $C_{15}H_9N^+$				**N-ovalene cations, $C_{31}H_{14}N^+$**			
1'N	3.49	0.00	3.49	1N	7.10	0.98	7.17
				1'N	5.38	4.81	7.21
N-benz[a]anthracene cations, $C_{17}H_{11}N^+$				1"N	4.92	4.26	6.51
1N	1.63	1.48	2.20	1'''N	0.00	3.47	3.47
1'N	2.09	4.92	5.35	2N	5.25	1.19	5.38
				2'N	1.59	3.65	3.98
N-chrysene cations, $C_{17}H_{11}N^+$				3N	4.32	1.02	4.44
1N	3.72	0.04	3.72	3'N	1.29	1.99	2.37
1'N	3.61	2.22	4.24	4N	0.00	1.56	1.56
1'''N	0.08	2.17	2.17				
				N-circum-circumcoronene cations, $C_{95}H_{24}N^+$			
N-coronene cations, $C_{23}H_{11}N^+$				2N	10.12	0.33	10.13
1N	5.48	0.19	5.49	2'N	9.09	0.00	9.09
2N	3.69	0.00	3.69	3N	7.47	1.94	7.72
3N	2.67	0.00	2.67	3'N	8.31	0.00	8.31
				4N	7.33	0.63	7.72
N-circumcoronene cations, $C_{53}H_{14}N^+$				5N	4.75	0.62	4.79
1N	9.23	0.23	9.23	6N	3.06	0.00	3.06
1'N	6.99	0.00	6.99	7N	2.54	0.00	2.54
2N	6.77	0.47	6.79				
3N	5.30	1.20	5.43				
4N	4.55	0.00	4.55				
5N	1.32	0.00	1.32				

4. The Near-IR Spectroscopy of PAHs and PANHs

Broadening the scope of our discussion to encompass the whole population of interstellar PAHs (N-bearing or otherwise) that dominate the mid-IR emission and turning our attention to shorter wavelengths, there is another aspect of the astrophysical problem that has emerged in recent years that warrants consideration here. While significant effort has been made to understand the global infrared spectral properties of PAHs under conditions appropriate to the emission zones, significantly less attention has been directed toward understanding their overall UV, Visible, and Near-IR (UV/Vis/NIR) spectral properties. Until recently, most experimental and theoretical studies of the electronic spectroscopy of PAHs and PAH ions in the UV/Vis/NIR regions have focused on specific bands in narrow wavelength regions to test the hypothesis that PAHs are responsible for some of the discrete diffuse interstellar bands (DIBs, e.g., Salama *et al.* 1996; Brechignac and Pino 1999; Biennier *et al.* 2003; Hirata *et al.* 2003 – references 22 through 49).

To remedy this situation, Mattioda *et al.* (2005a,b) measured the electronic spectra of many PAH ions, focusing on transitions in the NIR, the region least studied. This work stressed the importance of the oft-neglected point that PAH ions indeed have NIR transitions that warrant consideration when evaluating the interstellar radiation field. Mattioda *et al.* show that the PAH IR emission features can be pumped by NIR photons and that PAHs should impose broadband structure on the NIR portion of the extinction curve. Due to space limitations here we only briefly describe the role NIR photons play in pumping the IR emission features.

Since the IR emission bands were initially found to be associated with UV rich objects, and PAHs were known to absorb most strongly in the UV, it was tacitly assumed that they were pumped primarily by UV photons. However subsequent measurements showed that UV flux alone was insufficient to pump the measured intensities of the IR emission bands in certain objects, seeming to pose a problem for the PAH model (Aitken & Roche 1983; Uchida, Sellgren, & Werner 1998; Uchida *et al.* 2000). While it is well known that small neutral PAHs have a steep and sharp absorption cutoff in the UV with much weaker absorption extending into the visible, this cutoff smoothly moves to longer wavelength with increasing PAH size (e.g., Birks 1970; Malloci, Mulas, & Joblin 2004). Since this absorption characteristic of neutral (closed shell) species was incorporated in most PAH emission models (Schutte *et al.* 1993; Draine and Li, 2001; Li & Draine 2001; Bakes *et al.* 2001) these models could not account for observations of the IR bands from UV poor objects. However, upon ionization the neutral PAH electronic configuration changes from closed- to open-shell (radical) and moderate-to-strong absorptions occur at much longer wavelengths.

Taking this into account, Li & Draine (2002) extended their model and showed that ionized PAHs could indeed account for the IR emission features in these objects. Since the number of near-IR PAH ion experimental spectra available upon which to extend their model was severely limited, Li & Draine adopted the Desert *et al.* (1990) cutoff. However, the experimental measurements of Mattioda *et al.* (2005a,b) showed that this cutoff greatly underestimated PAH ion NIR absorption strengths and band widths. To properly take the role of NIR radiation into account, Mattioda *et al.* (2005b) extended Draine & Li's PAH UV/Visible formalism with their NIR experimental data and derived a model for the PAH ion absorption cross section spanning the FUV through the NIR.

With this model, Mattioda *et al.* (2005b) assess the amount of radiant energy PAHs absorb in the UV, Vis, and NIR wavelength regions individually and as function of stellar type. Figure 4 summarizes these results. The figure presents the UV through NIR blackbody stellar output for a variety of different star types, the model PAH ion absorption function and the convolution of the two. The integrated amount of radiant energy absorbed by these PAHs is indicated by the shaded areas in Figure 4 labeled: UV, Vis, and NIR. While the convolved function represents the amount of energy absorbed per carbon atom per wavelength, the area gives the total amount of radiant energy absorbed per C atom.

From the convolved curves in Figure 4 one can clearly see that as stellar temperature decreases, the amount of energy absorbed by PAH ions in the NIR relative to the amount absorbed in the UV and Visible increases markedly. Analysis of the curves shows the power absorbed in the NIR becomes nearly equivalent to the power absorbed in the UV and Visible for stellar temperatures around 4,000 K and 3,000 K respectively. For stars with lower stellar temperatures the NIR power absorbed exceeds that in the UV and Vis. These crossover temperatures are lower limits as the stellar radiation fields were derived asuming a blackbody radiation field. Using Kuruscz models reduces the UV output substantially with respect to the Vis and NIR, especially for early type stars.

Thus, while the availability of UV-Vis photons to pump the PAH emission features drops with decreasing star type, the contribution by the stellar NIR photons remains steady and actually becomes comparable to that of the higher energy photons for the later type stars. Inspection of the integrated power curves in Figure 4 shows that the net effect of decreasing stellar temperature is a steady but slow and gradual decrease in the integrated radiative power pumped into the PAH ions and a concomitantly slow decrease in the power emitted in the mid-IR by the PAH bands, not a precipitous drop as previously expected. This predicts that, if present in the vicinity of even very late
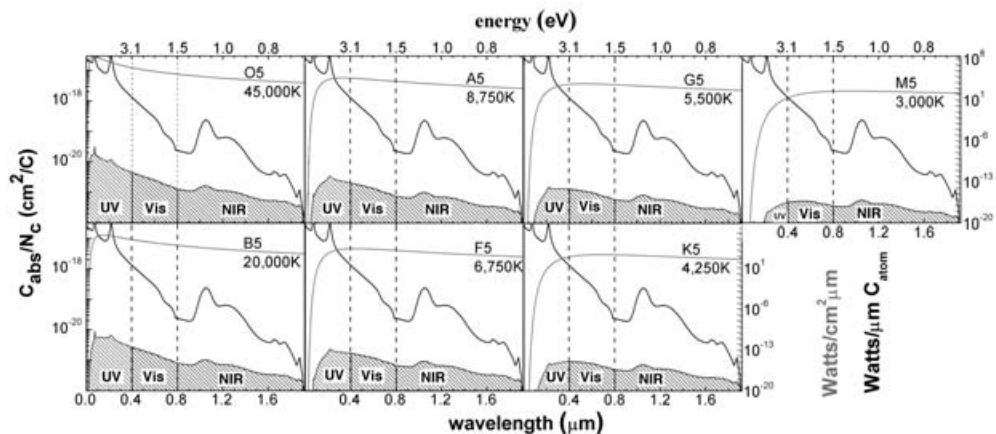
Figure 4. Stellar radiative energy absorbed by PAHs as a function of star type. The UV through NIR stellar (black body) output for a variety of different star types (smooth gray curve, right axis units: Watts/cm^2/μm) is plotted in conjunction with PAH ion absorption cross-section (structured curve, left axis units). The integrated amount of radiant power absorbed by an optically thick cloud of PAH ions is indicated by the shaded areas labeled UV, Vis, and NIR (right axis units: Watts/μm/Catom). PAH ion UV-Vis absorption is modeled using the Li & Draine (2002) formalism and NIR absorption is modeled using the formalism described in Mattioda *et al.* 2005b. Figure adapted from that reference. The vertical lines at 0.4 μm and 0.78 μm separate the spectral domains.

type stars, open shell PAH species (PAH ions and PANHs with an odd number of N atoms) can be vibrationally excited by the stellar radiation field. A much more detailed discussion can be found in Mattioda *et al.* (2005a).

Acknowledgements

References

Aitken, D.K. & Roche P.F. 1983, *MNRAS* 202, 1233

Allamandola, L.J., Hudgins, D.M., & Sandford, S.A. 1999, *Ap. J.* 511, L115

Allamandola, L.J., Tielens, A.G.G.M., & Barker, J.R. 1989, *Ap. J. Supp.* 71, 733

Bakes, E.L.O., Tielens, A.G.G.M., & Bauschlicher, C.W. 2001, *Ap. J.* 556, 501

Bakes, E.L.O., Tielens, A.G.G.M., Bauschlicher, C.W., Hudgins, D.M., & Allamandola, L.J. 2001, *Ap. J.* 560, 261.

Bauschlicher, C.W. & Langhoff, S.R. 1997, *Spectrochim. Acta A* 53, 1225

Biennier, L., Salama, F., Allamandola, L.J., & Scherer, J.J. 2003, *J. Chem. Phys.* 118, 7863

Birks, J.B. 1970, *Photophysics of Aromatic Molecules* (London: Wiley-Interscience)

Brechignac, P. & Pino, T. 1999, *A&A* 343, L49

Cox, P. & Kessler, M.F. (eds.), 1999 *The Universe as Seen by ISO, vol. I, II* (ESTEC, Noordwijk, The Netherlands: ESA Pub. Div.)

Desert, F.X., Boulanger, F., & Puget, J.L. 1990, *A&A* 237, 215

Draine, B.T. & Li, A. 2001, *Ap. J.* 551, 807

Hirata, S., Head-Gordon, M., Szczepanski, J., & Vala, M. 2003, *J. Phys. Chem. A* 107, 4940

Hony, S. *et al.* 2001, *A&A* 370, 1030

Hudgins, D.M. & Allamandola, L.J. 1995, *J. Phys. Chem.* 99, 3033

Hudgins, D.M. & Allamandola, L.J. 1999, *Ap. J.* 513, L69

Hudgins, D.M., Bauschlicher, C.W., & Allamandola, L.J. 2005, *Ap. J.* 632, 316

Joblin, C., Boissel, P., Leger, A., d'Hendecourt, L.B., & Defourneau, D. 1995, *A&A*, 299, 835

Kim, H.-S. & Saykally, R.J. 2002, *Ap. J. Supp.* 143, 455

Langhoff, S.R. 1996, *J. Phys. Chem.* 100, 2819

Li, A. & Draine, B.T. 2001, *Ap. J.* 554, 778

Li, A. & Draine, B.T. 2002, *Ap. J.* 572, 232

Malloci, G., Mulas, G., & Joblin, C. 2004, *A&A* 426, 105

Mattioda, A.L., Hudgins, D.M., Bauschlicher, C.W., Rosi, M., & Allamandola, L.J. 2003, *J. Phys. Chem. A* 107, 1486

Mattioda, A.L., Allamandola, L.J., & Hudgins, D.M. 2005a, *Ap. J.* 629, 1183

Mattioda, A. L., Hudgins, D.M., & Allamandola, L.J. 2005b, *Ap. J.* 629, 1188

Oomens, J., Tielens, A.G.G.M., Sartakov, B.G., von Helden, G., & Meijer, G. 2003, *Ap. J.* 591, 968

Pauzat, F. & Ellinger, Y. 2001, *MNRAS*, 324, 355

Pech, C., Joblin, C., & Boissel, P. 2002, *A&A* 388, 639

Peeters, E. *et al.* 2002, *A&A* 390, 1089

Puget, J.L. & Leger, A. 1989, *ARAA* 27, 161

Salama, F., Bakes, E., Allamandola, L.J., & Tielens, A.G.G.M. 1996, *Ap. J.* 458, 621

Schutte, W.A., Tielens, A.G.G.M., & Allamandola, L.J. 1993, *Ap. J.* 415, 397

Szczepanski, J., Drawdy, J., Wehlburg, C., & Vala, M. 1995, *Chem. Phys. Lett.* 245, 539

Uchida, K.I., Sellgren, K., & Werner M.W. 1998, *Ap. J.* 493, L109

Uchida,K.I., Sellgren,K., Werner,M.W., & Houdashelt, M.L. 2000, *Ap. J.* 530, 817

Vala, M., Szczepanski, J., Pauzat, F., Parisel, O., Talbi, D, & Ellinger, Y.J. 1994, *J. Phys. Chem.* 98, 9187

Van Kerckhoven, C. *et al.* 2000, *A&A* 357, 1013

Verstraete, L. *et al.* 2001, *A&A* 372, 981

Discussion

MCCALL: You have suggested that a very large number of species and a very large number of isomers are necessary to explain the unidentified infrared bands, and expressed some pessimism about the identification of individual PAHs. Does this imply that PAHs are poor candidates for the carries of the Diffuse Interstellar Bands, which are relatively few in number?

HUDGINS: I am surprised by the comment that the DIBs are "relatively few in number." It is my understanding that in excess of 300 DIBs of all shapes and sizes have been cataloged. Far from being a challenge to the PAH/DIB theory, I think that the richness of the DIP spectrum implies a large and diverse population of molecules-entirely consistent with the PAH/DIB theory. Also, while the interstellar PAH (PANH?) population is undoubtedly made up of a distribution of countless discrete molecular species, they will certainly not all be present in equal abundance. Therefore, not every single species in the population need be represented among the DIBs – only those members of the population that are present in sufficient abundance to produce a measurable absorption.

Snow: You have shown that the 6.2 μm UIR is matched best by a PANH mix, with an interior nitrogen atom substitution in place of a carbon atom. I find this, including the implications for the cosmic nitrogen budget, fascinating. But how does this nitrogen substitution affect the other UIRs?

Hudgins: Since the N-involved vibrations of PANH molecules blend effectively with the other vibrations of the carbon skeleton (CC stretches, bends) PANHs do not have any distinctive spectral features that would otherwise distinguish them from ordinary PAHs. The impact of N-substitution in PAHs is actually quite subtle. The small but significant blue shift of the dominant CC stretching band is at this point the only consistent, measurable effect that distinguishes the spectra of PAHs and PANHs.